International Journal of Solids and Structures 50 (2013) 3332–3338

Contents lists available at SciVerse ScienceDirect

International Journal of Solids and Structures

journal homepage: www.elsevier.com/locate/ijsolstr

Size effect on mechanical behavior of random fiber networks

A.S. Shahsavari, R.C. Picu *

Department of Mechanical, Aerospace and Nuclear Engineering, Rensselaer Polytechnic Institute, Troy, NY 12180, United States

ARTICLE INFO

Article history:
Received 22 October 2012
Received in revised form 3 May 2013
Available online 14 June 2013

Keywords:
Fiber networks
Size effect
Heterogeneous materials
Elasticity

ABSTRACT

Bonded random fiber networks are heterogeneous on multiple scales. This leads to a pronounced size effect on their mechanical behavior. In this study we quantify the size effect and determine the minimum model size required to eliminate the size effect for given set of system parameters. These include the network density, the fiber length and the fiber bending and axial stiffness. The results may guide the definition of models and the selection of the size of representative volume elements in sequential multiscale models of fiber networks. To underline the origins of the size effect, we characterize the network heterogeneity by analyzing the geometry of the network (density distribution), the strain field and the strain energy distribution. The dependence of the heterogeneity on the scale of observation and system parameters is discussed.

© 2013 Elsevier Ltd. All rights reserved.

1. Introduction

Fiber networks are a common occurrence in the natural and engineering worlds and generally play a structural role. These can be divided in bonded and non-bonded, fibers being bonded to each other at all or some contact points in bonded networks. In non-bonded networks fibers cannot cross, and interact only via topological constraints. The non-bonded networks can be further divided in woven and non-woven. The woven networks which have some degree of regularity/periodicity, are artificial constructs and are used in the textile and composite industries. Non-wovens are materials made from long, entangled fibers, with random distribution of their centers of mass and random spatial orientation, which stay together due to topological interactions and friction. Random fiber networks are present at all scales in the human and animal bodies. Most connective tissue, such as cartilage, tendon and ligaments, and the cornea, are made from collagen fiber networks. On the scale of individual cells, the cytoskeleton is a large random fiber network made from F-actin and in which fibers are densely cross-linked. This network has structural role and mediates signaling and transport of molecules in the cell (Mofrad, 2006; Jeffery et al., 1991; Riesle et al., 1998).

This broad range of applications led to a significant activity targeting primarily bonded networks. The goal of the first models was to predict the global material behavior based on few microstructural parameters such as the density and the fiber orientation (Algar, 1965; Astrom et al., 1994; Lee and Carnaby, 1992; Wu and Dzenis, 2005). These models were based on the assumption that deformation is affine, i.e. the local strains are identical to the global strains. With this assumption, and using the probability distribution function (PDF) of fiber orientations, it is possible to predict the elastic moduli of the ensemble of fibers. This approach is imperfect due to the fact that, in a range of network densities, such systems actually deform non-affinely (Head et al., 2003; Wilhelm and Frey, 2003; Hatami-Marbini and Picu, 2008). The degree of non-affinity depends on the scale of observation, being more pronounced as the system deformation is probed on smaller and smaller scales (Head et al., 2003; Hatami-Marbini and Picu, 2008). The non-affine deformation leads to a softer response on the system scale compared to what the affine approximation predicts (Chandran and Barocas, 2006; Heussinger and Frey, 2006). The inability of the affine models to correctly predict the system scale elasticity has triggered experimental and modeling activities aimed at understanding various aspects of the physics of deformation on sub-scale levels (Head et al., 2003; Wilhelm and Frey, 2003; Hatami-Marbini and Picu, 2008; DiDonna and Lubensky, 2005; Heussinger and Frey, 2007). The degree of non-affinity was quantified using various measures (Head et al., 2003; Leonforte et al., 2004; Onck et al., 2005; Hatami-Marbini and Picu, 2008) and it was shown to depend on the system density (fiber number density or mass density of the network). Sparse networks deform more non-affinely than dense networks. Despite the insight obtained from these studies, a mechanistic model predicting the elasticity of the material based on microstructural parameters and deformation mechanisms is not available.

In this article the heterogeneity of bonded networks is studied by computational means. The heterogeneity is described in terms of the geometry (based on density) and in terms of strain and strain energy evaluated on network sub-scales. The fluctuations of the density and strain field have been described in the literature function of the scale of observation in the context of non-affinity (Head

* Corresponding author. Tel.: +1 (518) 276 2195; fax: +1 (518) 276 6025.
E-mail address: picuc@rpi.edu (R.C. Picu).

0020-7683/$ - see front matter © 2013 Elsevier Ltd. All rights reserved.
http://dx.doi.org/10.1016/j.ijsolstr.2013.06.004

et al., 2003; Hatami-Marbini and Picu, 2008; Picu, 2011). The fluctuations of strain energy have not been described so far. The heterogeneity leads to a strong size effect affecting the network moduli. We study this size effect for several boundary conditions and prescribe rules by which a size effect-free model can be developed. This discussion also sheds light on the selection of representative volume elements in multiscale models of fiber networks.

2. The model, internal length scales and system parameters

The systems considered here are two dimensional networks generated by depositing fibers of length L_0 in a square domain of dimensions L, with random fiber orientation and centroid positions. Cross-links are introduced at all points where fibers intersect. The resulting structure is stress-free. The coordination, i.e. the number of neighboring cross links to which a given cross-link is connected, is at most $z = 4$ at all nodes, since no three fibers cross exactly at the same location. If the cross-links are modeled as pin joints, fibers are loaded by axial forces only. It has been shown that a 2D network of trusses with average coordination number $z < 4$ does not have rigidity and hence does not store mechanical energy (Kellomäki et al., 1996). If the cross-links are modeled as "welded" or "rotating" joints, the fibers are loaded both axially and in bending and the structure has non-vanishing stiffness even for $z = 4$. A rotating joint transfers bending moments along a given fiber but not between the two fibers joined at the respective cross-link. The angles between the intersecting fibers are preserved during deformation when the cross-link is modeled as a welded joint. This allows for moment transfer between fibers. In this work we consider rotating joints. The selection of rotating joints may be justified based on modeling arguments in some cases. An example is provided by the cellular cytoskeleton in which the F-actin fibers are linked by binding proteins (e.g. scruin) which transfer forces between fibers, but do not transfer bending moments. We note that using welded joints in place of the rotating joints leads to small numerical differences, but leaves the main conclusions unchanged. This is discussed in other publications (Wilhelm and Frey 2003; Heussinger and Frey 2007; Shahsavari and Picu, 2012).

Loading is imposed by specifying displacements along the boundary of the domain. Most results presented here, unless stated otherwise, are obtained for uniaxial far-field deformation ($\sigma_{11} = 0; \sigma_{22} \neq 0; \sigma_{12} = 0$). The dangling ends (the two end segments of each fiber which are connected to a single cross link) are excluded from the model because have no contribution to the energy of the system. Periodic boundary conditions are used in some simulations as specified in the text. When periodic boundary conditions are used, the structure has to fulfill the periodicity condition along the respective boundaries of the model. If a fiber crosses an edge, the portion of the fiber falling outside the domain is placed back in, on the opposite side. The imposed displacements and the periodic boundary conditions lead to non-zero forces and moments along the entire boundary, however the mean normal and shear stresses on faces perpendicular to the x_1 direction are kept zero.

The fiber material is considered linear elastic and fibers are characterized by the bending, axial and effective shear stiffness, $\kappa = E_f I$, $\eta = E_f A$ and $\gamma = \lambda G_f A$, respectively. A and I are the area and moment of inertia of the fiber cross-section, E_f is the fiber Young's modulus, G_f is the shear modulus, and λ is a constant which is taken here equal to 0.88 (for beams with circular cross section). The total energy of the system is the sum of the strain energies associated with bending, axial and shear deformation, i.e.

$$U = \frac{1}{2}\sum_{fibers}\int^{\kappa}\left(\frac{d\psi(s)}{ds}\right)^2 + \eta\left(\frac{du(s)}{ds}\right)^2 + \gamma\left(\frac{dv(s)}{ds} - \psi(s)\right)^2 ds. \qquad (1)$$

In this expression $v(s)$ represents the transverse displacement and $\frac{du(s)}{ds}$ is the axial strain at position s along the fiber. The rotation of the fiber cross-section is $\frac{dv(s)}{ds}$, while $\psi(s)$ represents the rotation of a plane which remains perpendicular to the neutral axis of the beam. Hence $\frac{dv(s)}{ds} - \psi(s)$ represents the shear deformation of the beam. Expression (1) corresponds to the Timoshenko model of the beam (Gere and Timoshenko, 1997). Note that the Euler–Bernoulli model is more often used for fibers. The two models give identical predictions for long, slender beams (beam length significantly larger than the cross-sectional dimension), while the Timoshenko model gives more accurate predictions for short beams. In random fiber-networks with random orientation of fibers, the distribution function of segment lengths is Poisson (Kallmes and Corte, 1960). Hence, a large number of short segments are present and, for given fiber diameter, one expects many segments to be too short to be modeled with the Euler–Bernoulli formulation. This motivates us to use the Timoshenko's model in this study (Shahsavari and Picu, 2012).

The solution of the network is evaluated by minimizing the total potential energy of the system using a finite element solver.

The system has the following characteristic length scales: the fiber length, L_0, centroid or fiber number density N, contour density $\rho = NL_0$, the mean segment length, l_c, and $l_b = (\kappa/\eta)^{1/2}$. The first two characteristic length scales result from the network structure, while l_b is related to the mechanical properties of individual filaments and denotes the relative importance of bending, κ, and axial stiffness, η. The fact that for this particular type of network the bending and axial stiffnesses appear in the constitutive law of the network only through a unique parameter, l_b, has been observed in Head et al. (2003) and Wilhelm and Frey (2003). For a cylindrical filament, l_b is equal to half of the cylinder radius. In this work these parameters were varied as follows: the system size $L/L_0 \in [5, 20]$ $l_b/L_0 \in [10^{-7}, 4 \times 10^{-2}]$ and the mean segment length $l_c/L_0 \in [0.005, 0.120]$. Note that for a network composed from fibers of constant length L_0, the mean segment length l_c is related to the fiber contour density ρ through the following relation (Kallmes and Corte, 1960):

$$l_c = \frac{\pi}{2\rho}. \qquad (2)$$

3. Results and discussion

The central objective of this article is to quantify the effect of the heterogeneity on the global properties of the network, and to provide quantitative information on the resulting size effect. To this end, the degree of heterogeneity is quantified first, and then its influence on the size effect of the elastic moduli is discussed. A method that can be used to infer the size of the model above which the small strain mechanical behavior is size-independent is presented in closure.

3.1. Characterization of network heterogeneity

By network heterogeneity we understand the variation of specific parameters across the problem domain, under loading conditions in which the respective parameters are expected to be position-independent if the material were a homogeneous continuum. A grid of characteristic size δ (composed from square elements of area δ^2), is overlaid on the problem domain and specific parameters are evaluated for each element. The parameters of interest are the density, the strain and the strain energy density.

The normalized density in each element, ρ, is computed as the total fiber length per element divided by δ^2 and by the nominal density of the system, ρ. Fig. 1 shows the probability distribution

function (PDF) of $\bar{\rho}_\delta$, $p(\bar{\rho}_\delta)$, for two systems, with $N = 200$ and $N = 600$ fibers per unit area, with $L_0 = 0.5$. The curves are obtained by probing with $\delta = 10l_c$ and $50l_c$. The mean segment length l_c is 0.015 and 0.005 for the two systems. Note that the distribution of segment lengths, $p(l)$, is Poisson and hence it is fully defined by its first moment, l_c (Kallmes and Corte, 1960). As expected, the distribution is narrower when δ is large and becomes broad when δ approaches the characteristic length l_c. The PDFs for the two densities coincide, which is a consequence of the stochastic process by which all these networks are generated.

The density is spatially correlated when $\delta \leqslant L_0$ (Hatami-Marbini and Picu, 2009). The correlations are due to the fact that a fiber spans a region of diameter L_0 around its centroid. The correlations have a range proportional to L_0 and a sharp cut-off beyond this distance. The functional form of this rather trivial correlation function can be obtained in close form (Dodson, 1971; Picu and Hatami-Marbini, 2010). Additional correlations may be introduced by the process of fiber deposition in a domain of finite size. These correlations decrease in range as the density increases, while the range of correlations introduced by the finite length of fibers is independent of density. The presence of correlations in the density field implies correlations in the effective moduli of the elements of the probing grid. A mapping from the discrete network model to a heterogeneous continuum with correlated elastic moduli which vary on length scales larger than δ was presented in Hatami-Marbini and Picu (2009).

Let us consider now the heterogeneity of the strain energy density distribution. To this end, consider three systems of different density and with different values of l_b. System I is characterized by $\rho = 100,\ L_0 = 0.5,\ l_b = 10^{-7}$, System II has fibers much stiffer in bending but same density, $\rho = 100,\ L_0 = 0.5,\ l_b = 10^{-3}$, and System III has large nominal density and large fiber bending stiffness, $\rho = 300,\ L_0 = 0.5,\ l_b = 10^{-3}$. All systems are loaded in uniaxial tension with 1% strain and the strain energy density is computed by summing up energies stored in the axial, bending and shear deformation modes of fibers. Let us denote the total energy per patch of size δ^2 by E_δ. This quantity, normalized by the mean value of the strain energy for a patch of same dimensions, is denoted by E_δ. Fig. 2 shows the PDF of E_δ for the three systems and for a probing length scale $\delta = 10l_c$ The PDFs are clearly distinct. The system with low density and small l_b exhibits the broadest distribution. This indicates that the degree of heterogeneity of the strain energy density is controlled by both ρ and l_b. Increasing l_b makes a relatively sparse system appear as homogeneous (compare systems I and II). This cannot be predicted exclusively based on the network geometry (Fig. 1).

A more direct way to visualize the heterogeneity of the energy distribution in the network is shown in Fig. 3. A realization of the

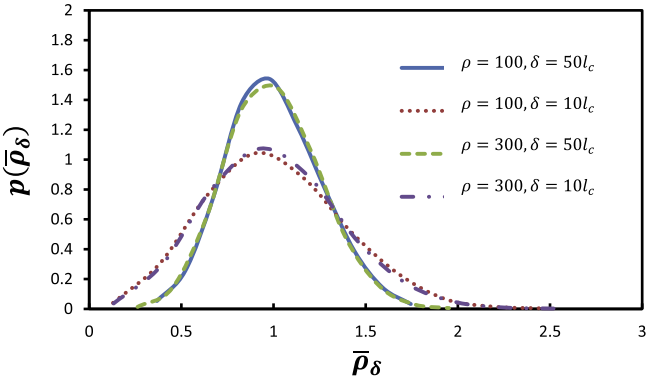

Fig. 1. Density PDFs at different probing scales, δ, and for networks of different nominal density, ρ.

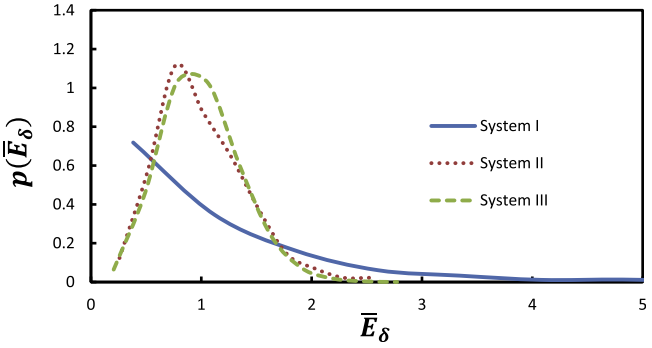

Fig. 2. Energy PDFs at probing scale $\delta = 10l_c$ for systems I–III defined in text.

network with $N = 200$ is considered, with the two values of l_b corresponding to systems I and II. The energy carried by each fiber segment in given system is ranked and the most loaded segments whose total energy amounts to 95% of the system strain energy are represented in black (dark). The others are represented in yellow[1] (light). Fig. 3(a) corresponds to system I and is mostly yellow (light); specifically, 15% of the fibers carry 95% of the strain energy. Fig. 3(b) corresponds to system II, and demonstrates a much more uniform energy distribution; 72% of the fibers carry 95% of the total energy. Note that if the deformation would be homogeneous, 95% of the fibers would carry 95% of the energy.

The heterogeneity may be also characterized based on the local strains measured on scale δ. The strain tensor associated with an element is computed by fitting linear functions, $u_1(x_1, x_2)$ and $u_2(x_1, x_2)$ to the displacements of all cross-links (nodes) in the respective sub-domain. The mean strain is evaluated from these functions using the small strain approximation of the Green strain. Fig. 4 shows the PDF of strain component ε_{22} (which is the non-zero component of the strain applied on the system scale) for networks I–III probed with $\delta = 10l_c$. The strain heterogeneity is very large in system I, with the local strain being negative, even though the equivalent global strain component is positive. This is in agreement with the observation in Hatami-Marbini and Picu (2008) where it was discussed that even when the global imposed strain has only one non-zero component (uniaxial), all local strain components and the components of the rotation tensor are non-zero. As with the strain energy, the distribution becomes narrower and the deformation appears more homogeneous when the density or/and l_b increase.

The physical picture emerging from this discussion is that of a material which resembles a heterogeneous continuum. If one accounts for variability from sample to sample, the effective equivalent continuum becomes stochastic, with strain energy sampled from the PDFs of Fig. 2. The degree of heterogeneity, characterized here by the second moment of these PDFs, is large for system I, but much smaller for systems II and III. Specifically, increasing the network density decreases the apparent heterogeneity of the fields. A more interesting effect is that the heterogeneity may be also reduced by increasing l_b at given network density and structure.

The purpose of this discussion on heterogeneity is to introduce the phenomena causing the size effect presented in Section 3.2.

3.2. Size effect

As discussed in the preceding section, the network model is characterized by its three independent parameters i.e. the density ρ, fiber length L_0 and the relative bending to axial stiffness of

[1] For interpretation of color in Figs. 3 and 6, the reader is referred to the web version of this article.

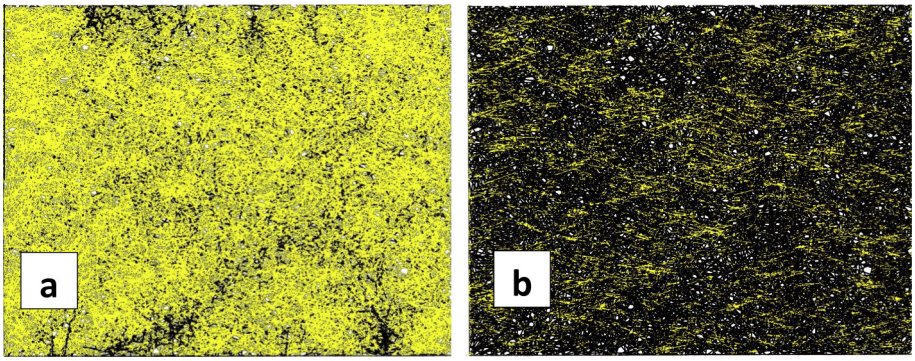

Fig. 3. Distribution of strain energy for two values of l_b. Fibers represented in black (dark color) carry 95% of the system strain energy. (a) corresponds to system I, while (b) corresponds to system II.

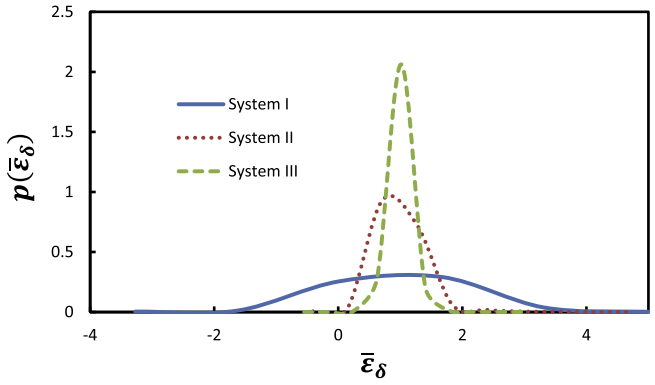

Fig. 4. PDFs of strain component ε_{22} at probing scale $\delta = 10l_c$ for systems I–III defined in the text.

constituent fibers, l_b. The size of the system, L, should be considered an additional length scale of the problem. To investigate the effect of the system size on the overall elastic modulus, E, networks with density $\rho = 50$ and $L_0 = 0.5$ and having different sizes are subjected to uniaxial tension while using periodic boundary conditions. Many realizations are produced and replica averaging is performed. The results of the size effect analysis are shown in Fig. 5. All curves converge to an asymptote at large L/L_0. The value of this asymptote, E_∞, is used to normalize the vertical axis for each system considered. The size effect depends strongly on system parameters, specifically, systems with fibers stiffer in bending exhibit a weaker size effect. This relates to the heterogeneity results discussed in Section 3.1. As l_b increases, the heterogeneity in all mechanical fields (strain, strain energy) decreases, which leads to a weaker size effect.

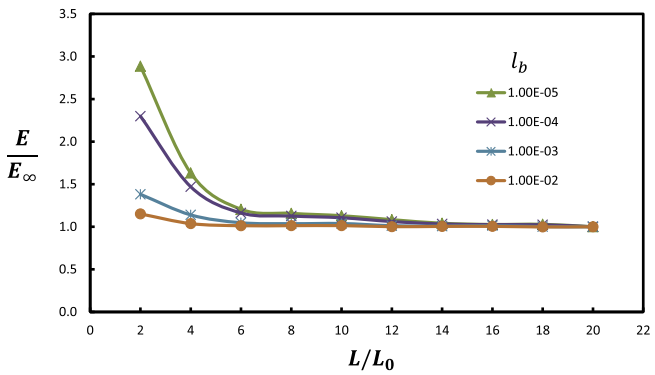

Fig. 5. Size effect of elastic modulus for different values of l_b and density $\rho = 50$.

The magnitude of the size effect is also investigated for various boundary conditions. The system with density $\rho = 50$ and $L_0 = 0.5$ is subjected to three types of boundary conditions shown in Fig. 6. These are color coded (also marked with different symbols) with the corresponding size effect curve. The size effect is evaluated for these three systems for two l_b values. Periodic boundary conditions are used for the systems shown in blue and green (diamonds and crosses), with the vertical edges of the model shown in blue (diamonds) being forced to remain straight during the deformation, and the vertical edges of the system shown in green (crosses) being free to deform. The normal stress in the horizontal direction is zero. Zero traction conditions are imposed along the vertical edges of the system shown in red (triangles) and no periodicity is enforced. The inferred Young's modulus of the network depends strongly on the type of boundary conditions applied. For the non-periodic system the convergence is from below, while for the two periodic systems the convergence is from above, which is in agreement with the behavior of a continuum model (Huet, 1990). The nature of the boundary conditions does not affect the rate of convergence and in the limit of large L all boundary conditions lead to the same effective moduli, as expected. As seen in Fig. 5, increasing l_b speeds-up the convergence of E to E_∞.

Because of the inherent stochasticity of the system, the elastic modulus varies from realization to realization. The variability from sample to sample decreases as the size of the system increases because a larger system includes more statistically independent subdomains. Another way of eliminating the effect of variability is performing replica averaging. The data shown in Figs. 5 and 6 corresponds to the mean of 25 realizations for each size and each system parameters. It is also important to note that for a given system size the variability depends on density and l_b.

3.3. Structure-properties relation: a master curve

We turn now to the effect of the system size on the inferred elastic constants of the network. To this end we repeat a scaling collapse analysis which led to a structure-properties-type constitutive relation (Head et al., 2003; Wilhelm and Frey, 2003), while using models large enough to eliminate any possible size and boundary conditions effects. Specifically, the system size is kept at least 10 times larger than the fiber length, and even larger, up to $20L_0$ for samples with low ρ and l_b. For each set of model parameters we consider 25 replicas.

Systems of various density, fiber length and l_b values are considered and their Young's modulus, E, and Poisson's ratio, ν, are evaluated numerically. The Young's modulus data are then collapsed to a master curve by proper normalization of the two axes (Head et al. 2003). Fig. 7 shows E function of ρ, L_0 and l_b. Data for 96 networks

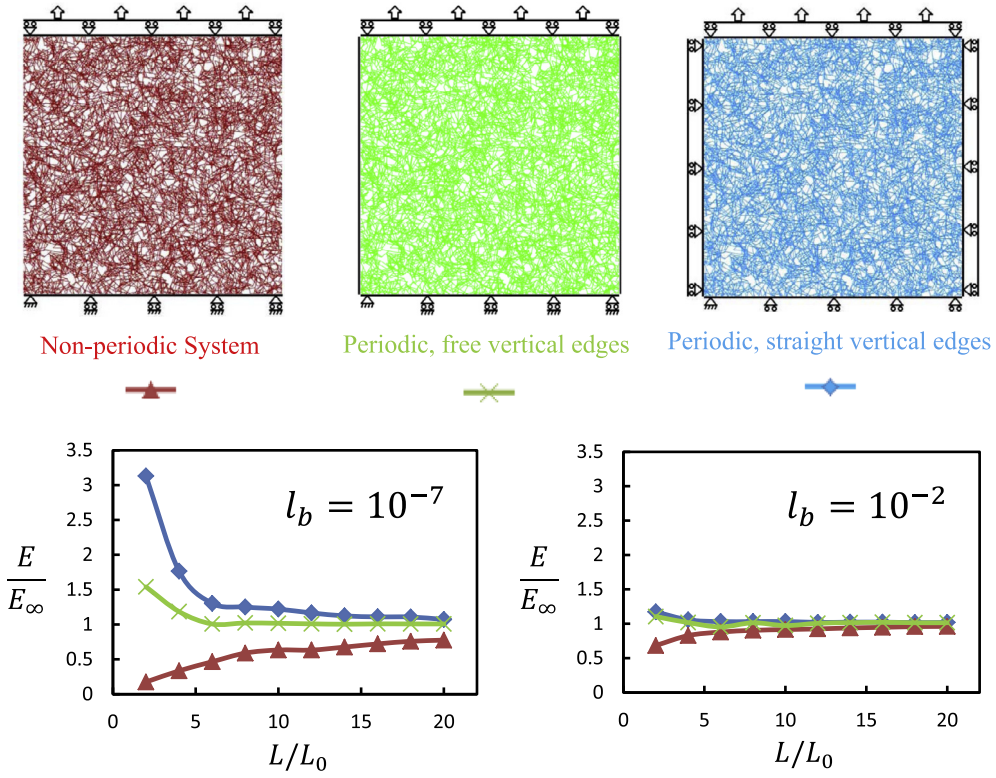

Fig. 6. Dependence of the size effect on boundary conditions. Results obtained by imposing three types of boundary conditions on the same network, at two values of l_b and for $\rho = 50$ are shown.

(sets of model parameters) with density ρ ranging from 50 to 300, fiber length L_0 ranging from 0.25 to 1, and l_b in the interval of $(10^{-7}, 10^{-2})$ are presented. The Young's modulus is normalized by $\rho\eta$ and a constant α which is a dimensionless quantity equal to 0.38. The variable of the horizontal axis is $w = (\rho L_0)^x (l_b/L_0)^y$. Note that according to Eq. (2), $\rho \sim l_c^{-1}$, i.e. $\rho L_0 \sim L_0/l_c$. The exponents x and y that provide data collapse on a master curve are $x = 7$ and $y = 2$. The curve reaches a plateau at large w. This indicates that the modulus is proportional to the density and to η. This dependence was inferred in the early network models where it was assumed that the deformation is affine (Wu and Dzenis, 2005; Lee and Carnaby, 1992) and was observed experimentally for paper (Rigdahl and Hollmark, 1986). Our results for this regime do not differ from those reported in the literature primarily because proper scaling can be obtained even with rather small systems.

At small w, the slope of the master curve in Fig. 7 is unity, hence the modulus is proportional to ρ^8, L_0^5 and to $\eta l_b^2 = \eta(\kappa/\eta) = \kappa$. The deformation in this regime is strongly non-affine and, as discussed in Section 3.2, the size effect is important. The exponents reported in the literature for this regime are slightly different. In Wilhelm and Frey (2003) and Heussinger and Frey (2007), the relation $E \sim \rho^{6.67}$ is inferred for the small w regime. In Head et al. (2003) the discussion is in terms of a length parameter, $\lambda = l_c(l_c/l_b)^q$, where L_0/λ is identical to parameter w used here. $q = 1/3$ gives the prefect collapse for the low density data which results in scaling of shear modulus as $G \sim E_f I \rho^9 L_0^6$, while at large densities, they

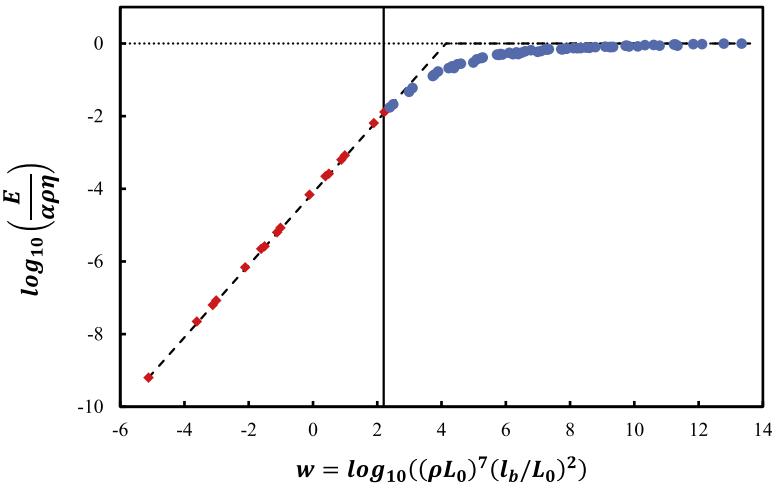

Fig. 7. Master plot providing the Young's modulus of the network as a function of system parameters. The data points correspond to 96 combinations of ρ, L_0 and l_b.

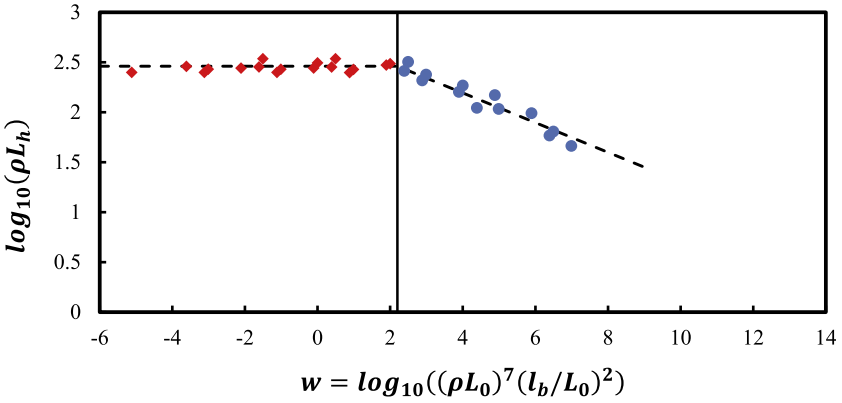

Fig. 8. Minimum model size which insures that the small strain mechanical behavior of the network is model size independent (within at most 10% error), L_h, in term of system parameters ρ, L_0 and l_b.

suggest $q = 2/5$, leading to $G \sim E_f I \rho^8 L_0^5$. We suggest that the size effect along with the use of different boundary conditions may lead to these apparently discrepant results. To substantiate this statement, let us consider that one evaluates the moduli for all values of w using the same model size, same boundary conditions and same number of replicas. The moduli are evaluated by averaging over all replicas of given system. In this case, the data points at large w would be more accurate than those at small w since the size effect is more pronounced in the non-affine regime. In addition, since a finite number of replicas is considered for each system, one has to account for the variability from sample to sample. The variability is more pronounced when smaller models are used and increases with decreasing w. Therefore, the data points in the non-affine regime have larger error bars than those corresponding to large w values. This uncertainty may lead to errors in the inferred slope and scaling exponent.

We emphasize that the master curve of Fig. 7 should be, in principle, free of size effects and sample to sample variability. In the limit of very large systems, eliminating the size effect also eliminates the variability. For the model sizes used to produce the data reported in Fig. 7 the variability is not entirely eliminated. The largest error bar is obtained for systems close to stiffness percolation (lowest w) and it is 6%. This is smaller than the size of the symbols in Fig. 7.

Finally, let us also mention that the large exponent of the scaling with the density, $E \sim \rho^8$, is specific to 2D models. Recent work (Broedersz et al., 2012) shows that networks in 3D are less sensitive to density and L_0, the shear modulus scaling in the non-affine regime as $G \sim \kappa \rho^3 L_0^2$.

3.4. Prediction of the scale of homogeneity

The present discussion has implications for the selection of the size of the smallest representative volume element (RVE) in sequential multiscale models of these structures, i.e. for identifying the "scale of homogeneity." Systems larger than this important length scale are free of size effects and their elastic constants are independent of the boundary conditions used for probing (provided these are such that would produce constant fields in a homogeneous sample). The value of L at which the modulus of systems shown in Fig. 6 converges to E_∞ is the minimum allowable RVE size.

To provide quantitative guidance for the selection of model sizes, we use data such as those in Fig. 5 and determine the model size, L_h, beyond which the modulus is within a range from the asymptote. The range is taken here to be 10%. L_h values are calculated using the most confining boundary conditions of Fig. 6. Therefore in practical situations, the error is expected to be less than 10%. L_h values are shown in Fig. 8 versus parameter w of the master curve in Fig. 7. Multiplying the vertical axis by the density, ρ, which is equivalent to the normalization of L_h by l_c (Eq. (2)), results in a reasonable collapse of the data. A clear demarcation is observed between systems with small w (red diamonds), which are characterized by large heterogeneity and strongly non-affine deformation, and those with w larger than approximately $10^{2.2} = 160$ (blue circles) which correspond to mostly affinely deforming networks. For $w < 160$ the scale of homogeneity, L_h, depends only on l_c as:

$$L_h \approx 180 l_c. \tag{3}$$

This indicates that L_h diverges as the percolation limit is approached from above due to the reduction of the density, and the system is in the non-affine deformation range of w. This is a known result. The present analysis provides a relationship defining this divergence and indicates that L_h is independent of L_0 in this range.

For systems with $w > 160$, L_h decays with increasing w. The slope of the best fit to the data in this range is -0.15 and hence one can write

$$L_h \sim 1/(\rho w^{0.15}) \sim l_c^2 L_0^{0.75} l_b^{0.3}. \tag{4}$$

The minimum model size should also be larger than any correlation length of the geometry or mechanical fields. As discussed in Section 3.1, fiber networks exhibit spatial correlations of range approximately equal to the fiber length, L_0. Therefore, L_h is bounded below by L_0 and this condition must be used in conjunction with Eqs. (3) and (4) (Fig. 8) to predict the smallest model and RVE size.

4. Conclusions

This article addresses several issues related to the heterogeneity of bonded networks, drawing a parallel between these systems and heterogeneous continua. The heterogeneity is described in terms of the network geometry (based on density) and in terms of strain and strain energy evaluated on sub-scales. The density heterogeneity depends primarily on the scale of observation. The energy and strain heterogeneity depend on ρ and l_b, with the heterogeneity decreasing as these parameters increase. The network shifts form a non-affinely deforming structure to an (approximately) affinely deforming one even when the density is kept constant and the bending stiffness of fibers increases relative to the axial stiffness.

The important result of this article is related to the size effect associated with network moduli. The pronounced heterogeneity described here leads to a strong dependence of the measured

moduli on the size of the probed network domain. We quantify this size effect and provide a simple relation linking the system parameters to the smallest model size which insures that the small strain mechanical response is model size independent.

References

Algar, W.H., 1965. Effect of structure on the mechanical properties of paper. In: Bolam, F. (Ed.), Consolidation of the Paper Web. Transactions of the Fundamental Research Symposium, Cambridge, pp. 814–849.

Astrom, J., Saarinen, S., Niskanen, K., Kurkijarvi, J., 1994. Microscopic mechanics of fiber networks. Journal of Applied Physics 75 (5), 2383–2392.

Broedersz, C.P., Sheinman, M., MacKintosh, F.C., 2012. Filament-length-controlled elasticity in 3D fiber networks. Physical Review Letter 108, 078102.

Chandran, P.L., Barocas, V.H., 2006. Affine versus non-affine fibril kinematics in collagen networks: theoretical studies of network behavior. ASME Journal of Biomechanical Engineering 128, 259–270.

DiDonna, B.A., Lubensky, T.C., 2005. Nonaffine correlations in random elastic media. Physical Review E 72, 066619.

Dodson, C.J.T., 1971. Spatial variability and the theory of sampling in random fibrous networks. Journal of Royal Statistical Society, Series B 33 (1), 88–94.

Gere, J.M., Timoshenko, S.P., 1997. Mechanics of Materials. Pws Pub.

Hatami-Marbini, H., Picu, R.C., 2008. Scaling of nonaffine deformation in random semiflexible fiber networks. Physical Review E 77, 062103.

Hatami-Marbini, H., Picu, R.C., 2009. Heterogeneous long-range correlated deformation of semiflexible random fiber networks. Physical Review E 80, 046703.

Head, D.A., Levine, A.J., MacKintosh, F.C., 2003. Distinct regimes of elastic response and deformation modes of cross-linked cytoskeletal and semiflexible polymer networks. Physical Review E 68, 061907.

Heussinger, C., Frey, E., 2006. Floppy modes and non-affine deformations in random fiber networks. Physical Review Letter 97, 105501.

Heussinger, C., Frey, E., 2007. Role of architecture in the elastic response of semiflexible polymer and fiber networks. Physical Review E 75, 011917.

Huet, C., 1990. Application of variational concepts to size effects in elastic heterogeneous bodies. Journal of Mechanics and Physics of Solids 38, 813–841.

Jeffery, A.K., Blunn, G.W., Archer, C.W., Bentley, G., 1991. Three-dimensional collagen architecture in bovine articular cartilage. Journal of Bone Joint Surgery 73 (5), 795–801.

Kallmes, O., Corte, H., 1960. The structure of paper. I. The statistical geometry of an ideal two dimensional fiber network. Tappi Journal 43, 737–752.

Kellomäki, M., Åström, J., Timonen, J., 1996. Rigidity and dynamics of random spring networks. Physical Review Letter 77, 2730–2733.

Lee, D.H., Carnaby, G.A., 1992. Compression energy of random fiber assembly. Part II: Theory. Textile Research Journal 62 (4), 185–191.

Leonforte, F., Tanguy, A., Wittmer, J.P., Barrat, J.L., 2004. Continuum limit of amorphous elastic bodies. II: Linear response to a point source force. Physical Review B 70, 014203.

Mofrad, M.R.K., 2006. Cytoskeletal Mechanics: Models and Measurements. Cambridge University Press.

Onck, P.R., Koeman, T., Van Dillen, T., van der Giessen, E., 2005. Rigidity and dynamics of random spring networks. Physical Review Letter 95, 178102.

Picu, R.C., Hatami-Marbini, H., 2010. Long range correlations of elastic fields in semi-flexible fiber networks. Computational Mechanics 46, 635–640.

Picu, R.C., 2011. Mechanics of random fiber networks – a review. Soft Matter 7, 6768.

Riesle, J., Hollander, P., Langer, R., Freed, L.E., Vunjak-Novakovic, G., 1998. Collagen in tissue-engineered cartilage: types, structure, and crosslinks. Journal of Cellular Biochemistry 71 (3), 313-278.

Rigdahl, M., Hollmark, H., 1986. Network mechanics. In: Bristow, J.A., Koleth, P. (Eds.), Paper Structure and Properties. Marcel Dekker, p. 241 (Ch. 12).

Shahsavari, A., Picu, R.C., 2012. Model selection for athermal cross-linked fiber networks. Physical Review E 86, 011923.

Wilhelm, J., Frey, E., 2003. Elasticity of stiff polymer networks. Physical Review Letter 91, 108103.

Wu, X.F., Dzenis, Y.A., 2005. Elasticity of planar fiber networks. Journal of Applied Physics 98, 093501.